Non-Orthogonal Multiple Access-Based Underwater VLC Systems in the Presence of Turbulence

Lina Bariah, *Senior Member, IEEE*, Mohammed Elamassie, *Senior Member, IEEE*, Sami Muhaidat, *Senior Member, IEEE*, Paschalis C. Sofotasios, *Senior Member, IEEE*, and Murat Uysal, *Fellow, IEEE*

***Abstract*—The promising potential of underwater applications in visible light communication (VLC) systems has recently gained considerable research attention, as an efficient technology for enabling high data rate, massive connectivity, and ultra-low latency. Different from indoor VLC, underwater wireless communications experience harsh environmental challenges, yielding a degraded performance. Non-orthogonal multiple access (NOMA) was introduced to enhance spectral efficiency and connectivity of underwater VLC communications. In this paper, we develop a mathematical framework to evaluate the performance of NOMA-enabled underwater VLC systems in the presence of turbulence. Specifically, we derive a closed-form expression for the outage probability of NOMA over lognormal channels, while considering the effect of path loss and turbulence. The derived analytical results with the corresponding numerical results demonstrate that the transmission distance between laser diode and sensor nodes (SNs) has a high impact on the outage performance of the SNs, due to the increased turbulence level with increased distance. Moreover, the presented results show the effect of the water type on the outage performance of the SNs and on the optimum values of the power coefficients.**

***Index Terms*—Non-orthogonal multiple access (NOMA), underwater, outage probability, visible light communication (VLC), turbulence, path loss.**

I. Introduction

FEW decades ago, the potential of underwater wireless communications (UWC) was confined to the military field, due to its inherent security feature. However, recently, UWC has become an active research area with broad civilian and commercial applications, such as underwater archaeology, gas and natural minerals exploration, navigation, and disaster precaution [1]. This is motivated by the notable advantages of UWC, which include reliability, cost efficiency, flexibility, and high data rate communications. In unguided water environment, UWC is conventionally realized by radio frequency (RF) or acoustic links, and recently hybrid acoustic-visible light communications (VLC) systems were introduced. Particularly, in hybrid acoustic-VLC underwater communications, acoustic waves are exploited to broadcast to a group of wireless sensors, while VLC links are employed to enable sensor-to-sensor communications. Despite the wide popularity of acoustic waves in UWC, its low transmission rate and severe delay limit the potential of UWC to satisfy the extremely high data rates and real-time massive data exchange requirements of the future sixth generation (6G) wireless networks [2]. Meanwhile, it was proven that RF links outperform acoustic waves in UWC systems in terms of smooth air-water interface transition and high tolerance to turbulence and turbidity [3]. Nevertheless, the high cost and energy consumption and the short transmission distance, given that RF waves can propagate only few meters in underwater environment, are the main drawbacks of RF UWC. Underwater wireless VLC was proposed as a promising alternative to acoustic and RF UWC, due to its envisaged capability to enable high speed communication with relatively negligible latency and increased capacity [4]. In optical communications, as the light propagates in underwater environment, the water absorbs the ultraviolet and the infrared. Accordingly, the visible light, specifically the blue and green spectrum, is the most appropriate wavelength for underwater communications [5]. This has been further confirmed experimentally by Gilbert *et al.* in 1966 [6] and paved the scientific way towards underwater visible light communication (UVLC) with a wavelength ranging from 450 nm to 550 nm.

In particular, the current research contributions have investigated UVLC system from different aspects, such as path loss channel modeling [7]–[11], turbulence channel modeling [12]–[17], physical layer and upper layer concerns [17]–[19], in addition to survey research works [20], [21].

Although extensive research efforts have been devoted to investigate underwater VLC systems, the current research has primarily focused a single user scenario. It is worth noting that massive connectivity is a key requirement for beyond 5G (B5G) networks, in which efficient multiple access schemes should be developed to accommodate the surge increase in the number of connected devices with diverse data rate requirements. In this regard,

Manuscript received November 22, 2021; revised December 15, 2021; accepted December 17, 2021. Date of publication December 28, 2021; date of current version January 17, 2022. *(Corresponding author: Lina Bariah).*

Lina Bariah is with the KU Center for Cyber-Physical Systems, Department of Electrical Engineering and Computer Science, Khalifa University, Abu Dhabi 127788, UAE (e-mail: lina.bariah@ieee.org).

Mohammed Elamassie and Murat Uysal are with the Department of Electrical and Electronics Engineering, Özyeğin University, Istanbul 34794, Turkey (e-mail: mohammed.elamassie@ieee.org; murat.uysal@ozyegin.edu.tr).

Sami Muhaidat is with the KU Center for Cyber-Physical Systems, Department of Electrical Engineering and Computer Science, Khalifa University, Abu Dhabi 127788, UAE, and also with the Department of Systems and Computer Engineering, Carleton University Ottawa, ON K1S 5B6, Canada (e-mail: muhaidat@ieee.org).

Paschalis C. Sofotasios is with the Center for Cyber-Physical Systems, Department of Electrical and Computer Engineering, Khalifa University, Abu Dhabi 127788, UAE, and also with the Department of Electrical Engineering, Khalifa University, Abu Dhabi 127788, UAE (e-mail: p.sofotasios@ieee.org).

Digital Object Identifier 10.1109/JPHOT.2021.3138723

non-orthogonal multiple access (NOMA) was introduced as an efficient RF technique to provide enhanced latency, spectral efficiency, and massive connectivity. Unlike conventional orthogonal multiple access schemes, NOMA allows multiple users to simultaneously utilize the available time and frequency resources, with a controlled level of inter-user interference [22]. Motivated by this, NOMA-enabled underwater sensor networks was proposed as an efficient multi-access paradigm to allow multiple SNs to communicate with gateway nodes, simultaneously. In particular, it was demonstrated that NOMA enjoys robust capacity performance in UVLC, in the presence of underwater optical turbulence [23]. It was further shown that NOMA has superior performance in underwater environments, compared to air [24].

A. Related Work

Although the research on NOMA-enabled underwater VLC systems is limited, there are few works which addressed the performance of such systems. The authors in [24] conducted an experimental study to investigate the error rate performance of NOMA in underwater VLC systems. The results in [24] demonstrated the improved performance of NOMA systems in underwater scenarios, compared to air scenarios. In [25], the authors investigated the effect of random receiver orientation, residual interference, and node location on the outage probability (OP) performance of two users cooperative NOMA VLC in underwater environment, where they employed a decode-and-forward relay to improve the performance of the far user. Moreover, in [26], the authors numerically investigated the coverage probability and cell capacity of NOMA users in underwater VLC system. It is worth highlighting that a thorough performance evaluation of the OP of point-to-point NOMA in UVLC systems, in the presence of turbulence, is missing in the open literature. Note that such a study is essential and lays down the foundation for the realization of various NOMA-assisted UVLC use cases, including, underwater data mining, software update in SNs, etc [27].

Motivated by this, in this paper, we evaluate the performance of NOMA in underwater VLC systems under the presence of turbulence. In specific, we derive a novel analytical expression for the outage probability to quantify the performance of NOMA under different turbulence scenarios. To the best of our knowledge, none of the reported works in the literature has evaluated the outage performance of point-to-point NOMA VLC in underwater scenarios.

The remainder of the paper is organized as follows. Section II presents the adopted signal and system models, including path loss and turbulence models. Outage probability closed-form expression is derived in Section III followed by the corresponding numerical and simulation results in Section IV. Finally, closing remarks are presented in Section V.

II. System Model

In this work, we consider a downlink UVLC power-domain NOMA system, where a single laser source communicates simultaneously with M underwater sensor nodes (SNs). As depicted in Fig. 1, the m^{th} node, $m = 1, 2, 3, \cdots, M$, is located at a distance of d_m from the laser source. In a such power-domain

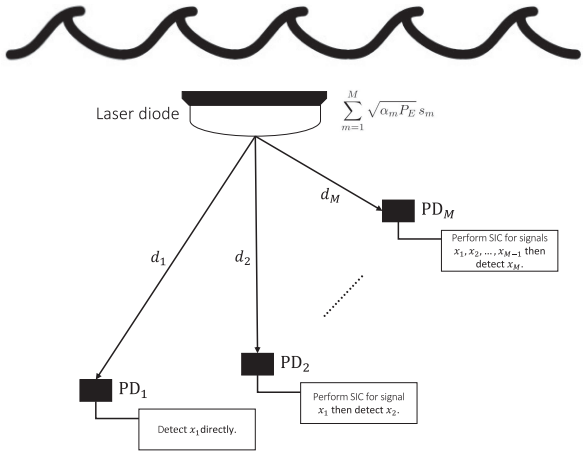

Fig. 1. NOMA for downlink UVLC.

NOMA system, power allocation coefficients are determined based on the channels conditions between the laser source and all receiving nodes (i.e., photo-detectors (PDs)) [22]. Particularly, close nodes to the laser source, which are nodes with strong channel coefficients, are allocated lower power coefficients. On the other hand, high power coefficients are considered for nodes with weak channels gains. Without loss of generality, we assume that channel gains are ordered in an ascending form, i.e., $h_M > h_{M-1} > \cdots > h_1$; hence, the power allocation coefficients can be written as $\alpha_1 > \cdots > \alpha_{M-1} > \alpha_M$. Since the highest transmit power is assigned to the first node, this SN will not perform successive interference cancellation (SIC). Meanwhile, the smallest power coefficient is allocated for the M^{th} node, and hence, this node will decode the data of $M-1$ nodes before decoding its own signal.

In this work, we consider both, deterministic path loss channel coefficient and turbulence induced fading. The path loss comprises the attenuation and the geometrical losses. It is worth noting that the effect of geometrical loss is negligible for the case of collimated light sources, while for diffused and semi-collimated sources, both of geometrical and attenuation loss should be considered [10]. In the current work, we consider semi-collimated laser sources. Different than laser sources with collimated beam, the spot of the received beam of a laser source with semi-collimated beam can provide the necessary coverage for a NOMA system, as depicted in Fig. 2.

A. Path Loss Model

Considering a line-of-sight (LOS) scenario, and under the assumption of transmitter-receiver perfect alignment, the path loss between the LD and the mth SN in underwater VLC scenario, for semi-collimated laser sources with Gaussian beam shape[1], can be modeled as [10]

$$g_m \approx \left(\frac{D_R}{\theta\, d_m}\right)^2 \exp\left(-q_t d_m \left(\frac{D_R}{\theta\, d_m}\right)^T\right), \tag{1}$$

[1]In this paper, we consider laser source with a Gaussian beam shape. It is worth highlighting that NOMA systems in UVLC have different performance when other distributions of beam shapes, such as the spherical and plane waves, are considered.

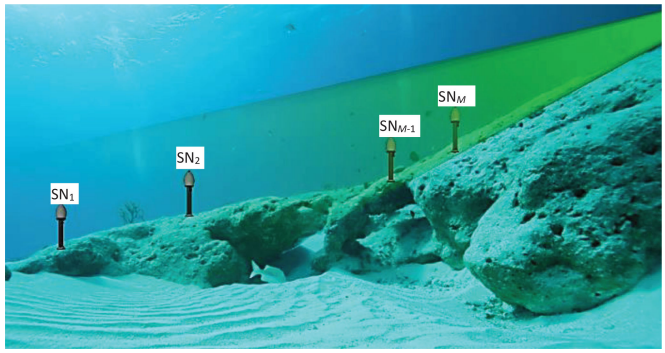

Fig. 2. The use of semi-collimated laser sources in underwater NOMA systems.

where d_m is the distance between the LD and the mth SN and D_R is the aperture diameter. Additionally, θ denotes the full width transmitter beam divergence angle, T is the correction coefficient, and q_t represents the extinction coefficient.

B. Turbulence Channel Model

The fading coefficient of the transmitter-receiver link is given by h_m, which represents the channel between the emitting LD and the mth SN. In this work, we consider that the probability density function (PDF) of h_m follows the log-normal distribution with mean μ_m and variance σ_m^2, and it is given by [28]

$$f_H(h_m) = \frac{1}{h_m\sqrt{2\pi\sigma_m^2}} \exp\left(-\frac{(\ln(h_m)-\mu_m)^2}{2\sigma_m^2}\right). \quad (2)$$

C. Signal Model

Following the NOMA principle, the LD broadcasts a superposed symbol comprising the summation of the weighted signals of the M SNs. Hence, the transmitted symbol at the single LD is given by $x = \sum_{m=1}^{M} \sqrt{\alpha_m P_E}\, s_m$, where P_E is the total transmitted optical power and α_m denotes the power allocation coefficient of the mth SN. Moreover, s_m represents the transmitted message of the mth SN. Without loss of generality, we assume that the average energy of transmitted symbols is normalized to unity. It is recalled that NOMA nodes are ordered based on their channel conditions. In specific, SNs with weak channel conditions are allocated higher power coefficients than SNs with stronger channel gains [22]. Therefore, without loss of generality, we assume that the first SN, SN_1, is the node with the weakest channel gain, while the Mth SN, SN_M, is the node with the strongest channel conditions. Subsequently, power coefficients are allocated such that $\alpha_1 > \alpha_2 > \cdots > \alpha_M$ and $\sum_{m=1}^{M} \alpha_m = 1$.

Therefore, the received signal at the mth NOMA receiver can be expressed as the following

$$y_m = \eta r g_m h_m x + n_m, \quad (3)$$

where n_m is the zero-mean additive white Gaussian noise (AWGN), and η and r denotes, respectively, the electro-optical conversion efficiency of the laser diode and the opto-electrical responsivity of the PD. According to NOMA, for M SNs scenario, channel gains are ordered as $h_1 < h_2 < \cdots < h_M$. Accordingly, power coefficients are assigned based on the channels ordering. Before attempting to detect its own signal, the mth SN should employ a SIC receiver to reduce the interference induced by signals with higher power levels, i.e., $x_1, \cdots, x_{m-1}$. Note that the interference caused by signals with lower power levels, i.e., $x_{m+1}, \cdots, x_M$, is less significant and will be treated as noise. Therefore, assuming perfect SIC, the output of the mth SIC receiver can be written as follows

$$y_m = \bar{g}_m h_m \left(\sqrt{\alpha_m P_E}\, s_m + \sum_{j=m+1}^{M} \sqrt{\alpha_j P_E}\, s_j\right) + n_m \quad (4)$$

where $\bar{g}_m = \eta r g_m$. Subsequently, the instantaneous signal-to-interference-plus-noise ratio (SINR) of the mth SN can be expressed as

$$\gamma_m = \frac{\bar{g}_m^2 h_m^2 \alpha_m P_E\, \mathcal{E}[|s_m|^2]}{\bar{g}_m^2 h_m^2 \sum_{j=m+1}^{M} \alpha_j P_E\, \mathcal{E}[|s_j|^2] + \mathcal{E}[|n_m|^2]}, \quad (5)$$

which can be rewritten as

$$\gamma_m = \frac{\alpha_m}{\sum_{j=m+1}^{M} \alpha_j + \frac{1}{\rho_m}}, \quad (6)$$

where ρ_m is the instantaneous signal-to-noise ratio (SNR) of the mth SN

$$\rho_m = P_E\, \bar{g}_m^2 h_m^2 / \sigma_n^2. \quad (7)$$

where σ_n^2 denotes the AWGN variance, and h_m^2 denotes the small-scale fading of the mth SN with PDF given by (2).

In the following, we analyze the outage probability of NOMA SNs in underwater VLC network.

III. Outage Probability Analysis

The outage probability metric is used to quantify the quality of service (QoS) of a wireless system and can be defined as the probability that the symbol error rate is greater than specific threshold. Analytically, outage probability can be evaluated as the probability that the SINR falls bellow a certain level. In this section, we analyze the outage probability of NOMA subject to the aforementioned path loss and turbulence models.

Proposition 1: The outage probability of the mth sorted NOMA SNs is evaluated as

$$P_{out,m} = \sum_{i=m}^{M} \sum_{k=0}^{M-i} \binom{M}{i} \binom{M-i}{k} (-1)^k \times \left[\frac{1}{2}\mathrm{erfc}\left(\frac{[\ln(\bar{\rho}_m) + 2\mu_m] - \ln(\varphi_j)}{\sqrt{8\sigma_m^2}}\right)\right]^{i+k} \quad (8)$$

where $\mathrm{erfc}(z) = 2/\sqrt{\pi}\int_z^{\infty} \exp(-t^2)dt$ denotes the error function [29],

$$\varphi_j = \max_{1\le j\le m} \frac{\phi_j}{\alpha_j - \beta_j \phi_j} \quad (9)$$

given that

$$\beta_j = \sum_{i=j+1}^{M} \alpha_i \tag{10}$$

and

$$\phi_j = 2^{\tilde{R}_j} - 1, \tag{11}$$

where $\tilde{R}_j$ is the targeted data rate of the jth SN. Moreover,

$$\bar{\rho}_m = P_E \, \bar{g}_m^2 / \sigma_n^2, \tag{12}$$

$\mu_m = 2\mu_x$, and $\sigma_m^2 = 4\sigma_x^2$, where μ_x and σ_x^2 denotes the mean and the variance of the log-amplitude $X = 0.5\ln(h_m^2)$. It is essential to highlight that (8) is valid for

$$0 \leq \phi_m \leq \alpha_m / \beta_m \tag{13}$$

otherwise, $P_{out,m} = 1$.

Using (8), the average OP of all NOMA SNs can be evaluated as $P_{out,avg} = (1/M) \sum_{m=1}^{M} P_{out,m}$.

Proof: The outage probability of the mth SN is computed as the probability that the mth SN cannot detect its own signal or the jth SN's signal, where $1 \leq j < m$, subsequently, the mth SN fails to perform successful SIC. Hence, the outage probability of the mth SN can be evaluated as

$$P_{out,m} = 1 - \Pr\left(E_{m,1}^c \bigcap \cdots \bigcap E_{m,m}^c\right), \tag{14}$$

where $E_{m,j}$ denotes the event that the mth SN cannot successfully detect the jth SN's signal, which is defined as $E_{m,j} \triangleq \{R_{m\to j} < \tilde{R}_j\}$, given that $R_{m\to j}$ is the mth SN rate to detect the jth SN signal. Additionally, $E_{m,j}^c$ denotes the complementary set of $E_{m,j}$, which can be written as [30]

$$\begin{aligned} E_{m,j}^c &= \left\{ \log\left(1 + \frac{\alpha_m}{\sum_{j=m+1}^{M} \alpha_j + \frac{1}{\rho_m}}\right) > \tilde{R}_j \right\} \\ &= \left\{ \frac{\alpha_m}{\alpha_j \beta_j + \frac{1}{\rho_m}} > \phi_j \right\}. \end{aligned} \tag{15}$$

Therefore, using (14) and (15) and after some mathematical manipulations, the outage probability of the mth SN can be written as

$$\begin{aligned} P_{out,m} &= 1 - \Pr\left(\rho_m > \varphi_j\right) \\ &= F_{\varrho_m}\left(\varphi_j\right) \end{aligned} \tag{16}$$

where $F_{X_m}(x)$ is the mth ordered cumulative distribution function (CDF) of the random variable X. Recalling that the instantaneous SNR of the mth SN is $\rho_m = \bar{\rho}_m h_m^2$ and h_m follows the log-normal distribution, the un-ordered CDF of ρ_m is given by [31]

$$F_{\varrho}(x) = \frac{1}{2}\text{erfc}\left(\frac{[\ln(\bar{\rho}) + 2\mu_m] - \ln(x)}{\sqrt{8\sigma_m^2}}\right). \tag{17}$$

Subsequently, utilizing order statistics, the mth ordered CDF of ρ_m can be written as (18), shown at the bottom of this page.

Inserting (17) into (18) and using binomial expansion, yield the outage probability of the mth SN as given by (8). □

IV. Numerical Results

In this section, we present numerical results to show the outage probability performance of the SNs in NOMA underwater VLC system with the presence of turbulence. Without loss of generality, we consider a two SNs scenario, $M = 2$, each equipped with a single PD. In specific, the first SN, SN_1, is the node with the weak channel gain, while the second SN, SN_2, is the node with the strong channel gain. Moreover, we investigated the performance of the underlying system model under two water types, namely, clear ocean and coastal water with extinction and correction coefficients (c, T) equals to (0.15,0.05) and (0.305,0.13), respectively [10], [32]. Also, we consider receiver aperture diameter of $D_R = 5$ cm and full width transmitter beam divergence angle $\theta = 6^\circ$. The noise variance is assumed $\sigma_n^2 = -120$ dBm and the total transmitted optical power is normalized to unity, $P_E = 1$. Additionally, the electro-optical conversion efficiency of the laser diode and the opto-electrical responsivity of the PD are set to $\eta = 0.5$ [33] and $r = 0.4$ [34], [35], respectively. Finally, assuming salinity of 35 PPT and temperature of 20°C, the variance σ_x^2 can be calculated by using $\sigma_x^2 = 0.25\ln(1 + \sigma_I^2)$ with σ_I^2 denoting the scintillation index[2] and can be calculated, for laser sources with Gaussian beam shape using [36, Eq. 7] in conjunction with [37, Eq. 16]. In order to compute σ_I^2, we assume the following. The dissipation rate of mean-squared temperature equals to $1 \times 10^{-3}\text{K}^2\text{s}^{-3}$, the dissipation rate of turbulent kinetic energy per unit mass of fluid equals to $1 \times 10^{-2}\text{m}^2\text{s}^{-3}$, relative strength of temperature to salinity fluctuation of ω = -3, and wavelength of $\lambda = 530$ nm [23], [37]. The relationship between the scintillation index and path-loss coefficients for clear ocean and coastal water is presented in Table I for different transmission distances.

The individual and average outage probability of the two SNs versus the average receive SNR are presented in Fig. 3, for different power coefficient values, $\alpha_1 = 0.6$ and 0.9. The average receive SNR is given by (12). The figure shows the effect of the power coefficient α_1 on the outage performance of the two SNs. Note that $\alpha_2 = 1 - \alpha_1$. It can be shown from Fig. 3 that although power coefficients highly affects the outage probability performance of each SN, changing the power coefficient values does not affect the achievable diversity order of NOMA SNs. This can be observed from the slope of the outage probability at high SNR values.

In Fig. 4, we present the individual and average outage probability of the two SNs versus the transmission distance for

[2]scintillation index is the normalized variance of the fluctuating intensity.

$$F_{\varrho_m}\left(\varphi_j\right) = \begin{cases} \sum_{i=m}^{M} \binom{M}{i} \left[F_{\varrho}\left(\varphi_j\right)\right]^i \left[1 - F_{\varrho}\left(\varphi_j\right)\right]^{M-i} & , 0 \leq \phi_m \leq \frac{\alpha_m}{\beta_m} \\ 1 & , \phi_m > \frac{\alpha_m}{\beta_m} \end{cases} \tag{18}$$

TABLE I
PATH-LOSS COEFFICIENTS AND SCINTILLATION INDEX FOR DIFFERENT DISTANCES

d_m (m)	20	21	22	23	24
g_m (Clear ocean)	0.4730×10^{-4}	0.3813×10^{-4}	0.3088×10^{-4}	0.2512×10^{-4}	0.2052×10^{-4}
g_m (Coastal water)	0.1335×10^{-4}	0.1029×10^{-4}	0.0798×10^{-4}	0.0622×10^{-4}	0.0486×10^{-4}
σ_I^2	0.2527	0.2912	0.3333	0.3791	0.4288
d_m (m)	25	26	27	28	29
g_m (Clear ocean)	0.1682×10^{-4}	0.1384×10^{-4}	0.1142×10^{-4}	0.0945×10^{-4}	0.0784×10^{-4}
g_m (Coastal water)	0.0382×10^{-4}	0.0302×10^{-4}	0.0239×10^{-4}	0.0190×10^{-4}	0.0152×10^{-4}
σ_I^2	0.4824	0.5401	0.6021	0.6684	0.7392
d_m (m)	30	31	32	33	34
g_m (Clear ocean)	0.653×10^{-5}	0.5445×10^{-5}	0.4553×10^{-5}	0.3814×10^{-5}	0.3202×10^{-5}
g_m (Coastal water)	0.1213×10^{-5}	0.0973×10^{-5}	0.0783×10^{-5}	0.0632×10^{-5}	0.0511×10^{-5}
σ_I^2	0.8146	0.8947	0.9796	1.0695	1.1643
d_m (m)	35	36	37	38	39
g_m (Clear ocean)	0.2693×10^{-5}	0.227×10^{-5}	0.1916×10^{-5}	0.162×10^{-5}	0.1371×10^{-5}
g_m (Coastal water)	0.0414×10^{-5}	0.0336×10^{-5}	0.0274×10^{-5}	0.0223×10^{-5}	0.0182×10^{-5}
σ_I^2	1.2643	1.3696	1.4802	1.5962	1.7178

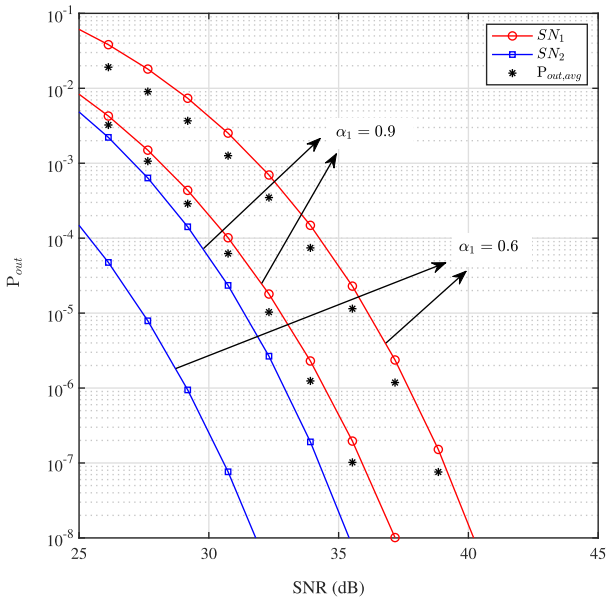

Fig. 3. First SN, second SN and average outage probabilities versus receive SNR, clear ocean, $\alpha_1 = 0.9$.

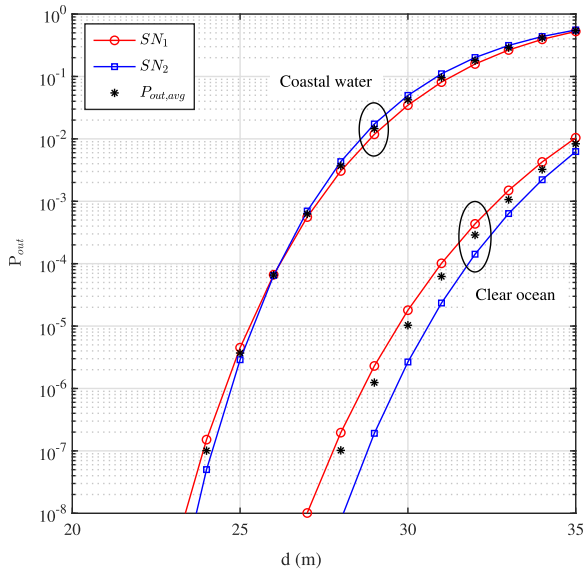

Fig. 4. First SN, second SN and average outage probabilities versus transmission distance for different water types, $\alpha_1 = 0.9$.

different types of water, namely, clear ocean and coastal water. It can be observed from the figure that in clear ocean scenario, the outage probability outperforms the coastal water scenario. This is due to the increased concentration of particulates in coastal water, compared to clear ocean, which act as scatterers and lead to severe signal attenuation. Moreover, it can be noticed from Fig. 4 that the distance between the PD and the SNs plays a significant rule in quantifying the outage performance of NOMA SNs. In particular, for a specific performance threshold, transmission distance can be selected to satisfy a certain QoS constraints. For example, for clear ocean scenario, given that the threshold value of the average outage probability is selected to be 10^{-10}, the maximum allowable distance between the laser source and any NOMA SN should not exceed 25.75 m.

The effect of power coefficients is demonstrated in Fig. 5, where the individual and average outage probability of the two SNs are plotted versus α_1 for clear ocean and coastal water scenarios, $d = 30$ m. Targeting users fairness, in which we aim to achieve an equivalent QoS levels for all nodes without prioritizing a particular node, it can be noticed from the figure that the type of water affects the optimum power coefficient value. In specific, it can be shown that the optimum power coefficient that yields fairness for the two SNs equals to 0.88 and 0.93 for coastal water and clear ocean, respectively. Apart from fairness, it can be observed that under particular system requirement and according

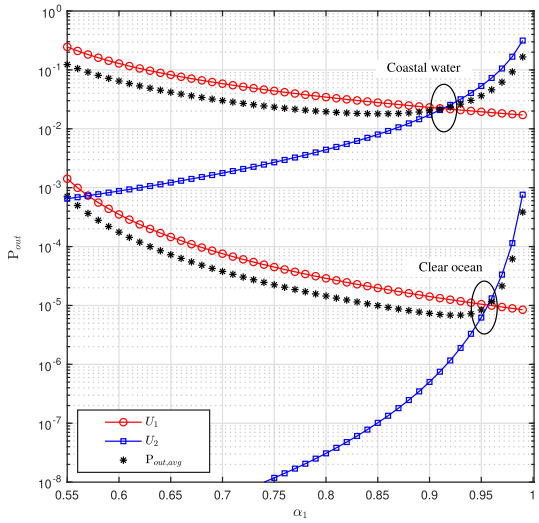

Fig. 5. First SN, second SN and average outage probabilities versus α_1 for different water types, $d = 30$.

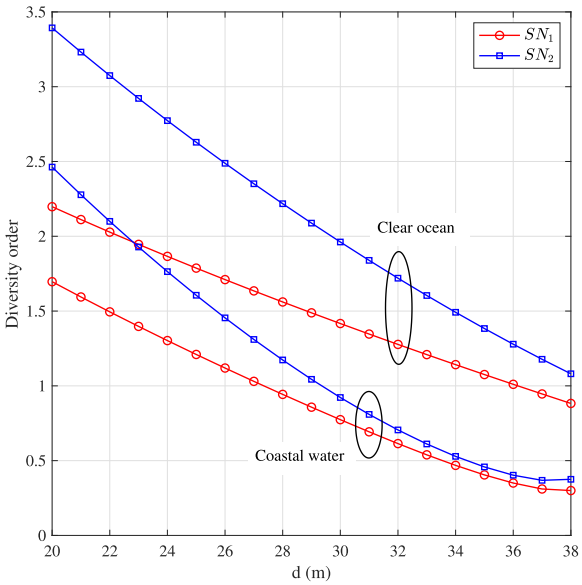

Fig. 6. The achievable diversity order of the two SNs versus the distance, for different water types.

to the turbulence model, power allocation coefficient can significantly affect the outage performance of NOMA underwater VLC systems. Therefore, efficient power allocation schemes should be developed in order to satisfy specific performance level.

Fig. 6 shows the effect of transmission distance and water type on the achievable diversity order of NOMA nodes. Note that the achievable diversity order is defined as the slope of the outage probability at high SNR values, and can be evaluated for the mth SN as follows

$$\text{Diversity} = -\frac{\log P_{out,m}}{\log \bar{\rho}_m}. \tag{19}$$

It can be observed from Fig. 6 that the water type significantly affects the outage performance of NOMA nodes in underwater VLC systems. For example, it can be noticed that at distance $d = 30$ m, the achievable diversity gain of the second SN equals

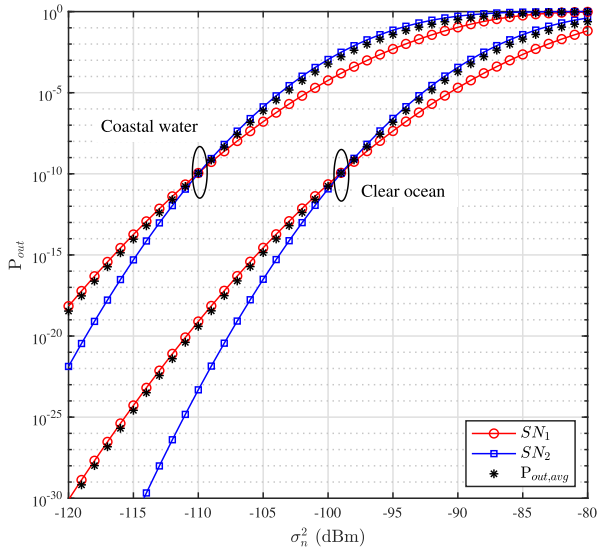

Fig. 7. The outage performance of the two SNs versus the different noise variance, $d = 20$ m, $\alpha_1 = 0.9$.

to 0.77 for the coastal water scenario, while for the clear ocean the diversity gain of the same node equals to 1.41. The same observation can be obtained for the first SN. Apart from the water type, it can be noticed that the transmission distance play an important role in quantifying the achievable diversity order of each SN, where it can be observed that, as the transmission distance increases from 20 m to 38 m, the diversity order decreases by 1.38 and 1.39, for clear ocean and coastal water scenarios, respectively.

Fig. 7 demonstrates the effect of the thermal noise variance on the OP performance of the two SNs, for clear ocean and coastal water scenarios. It can be observed from the figure that the effect of the noise power is more pronounced on the outage performance of nodes with lower power coefficients. This is even more evident in the coastal water scenario, where the increased number of scatters further attenuate the received signal strength, and hence, any change in the noise power level causes a detrimental effect on the outage performance of NOMA nodes.

V. Conclusion

In this work, we investigated the outage probability performance of NOMA SNs in underwater VLC system, under the assumption of turbulence. Particularly, we derived a novel analytical expression for the outage probability over log-normal turbulence model. From the derived analytical expression and the presented numerical results, it was observed that the transmission distance in addition to the water type highly affect the outage performance of NOMA SNs. Particularly, it was noticed that the outage probability of the SNs in clear ocean environment outperforms the ones in coastal water, due to the increased concentration of scatterers in the latter. Finally, it was shown from the obtained results that, although power coefficient allocation significantly affects the outage performance of all SNs, it has no effect on the achievable diversity order. Rather, the water type, as well as the distance, have direct impact on the diversity order of NOMA nodes in underwater VLC environment.

REFERENCES

[1] N. Anous, M. Abdallah, M. Uysal, and K. Qaraqe, "Performance evaluation of LOS and NLOS vertical inhomogeneous links in underwater visible light communications," *IEEE Access*, vol. 6, pp. 22408–22420, Mar. 2018.

[2] Z. Zeng, S. Fu, H. Zhang, Y. Dong, and J. Cheng, "A survey of underwater optical wireless communications," *IEEE Commun. Surv. Tuts*., vol. 19, no. 1, pp. 204–238, Jan.–Mar. 2017.

[3] X. Che, I. Wells, G. Dickers, P. Kear, and X. Gong, "Re-evaluation of RF electromagnetic communication in underwater sensor networks," *IEEE Commun. Mag*., vol. 48, no. 12, pp. 143–151, Dec. 2010.

[4] H. Lu *et al.*, "An 8 m/9.6 Gbps underwater wireless optical communication system," *IEEE Photon. J*., vol. 8, no. 5, Oct. 2016, Art. no. 7906107.

[5] S. Q. Duntley, "Light in the sea," *JOSA*, vol. 53, no. 2, pp. 214–233, 1963.

[6] G. Gilbert, T. Stoner, and J. Jernigan, "Underwater experiments on the polarization, coherence, and scattering properties of a pulsed blue-green laser," in *Underwater Photo Opt. I*, vol. 7. International Society for Optics and Photonics, 1966, pp. 8–14.

[7] C. Gabriel, M.-A. Khalighi, S. Bourennane, P. Léon, and V. Rigaud, "Monte-Carlo-based channel characterization for underwater optical communication systems," *J. Opt. Commun. Netw*., vol. 5, no. 1, pp. 1–12, 2013.

[8] S. Tang, Y. Dong, and X. Zhang, "On path loss of NLOS underwater wireless optical communication links," in *Proc. MTS/IEEE OCEANS-Bergen*, 2013, pp. 1–3.

[9] F. Miramirkhani and M. Uysal, "Visible light communication channel modeling for underwater environments with blocking and shadowing," *IEEE Access*, vol. 6, pp. 1082–1090, 2017.

[10] M. Elamassie, F. Miramirkhani, and M. Uysal, "Performance characterization of underwater visible light communication," *IEEE Trans. Commun*., vol. 67, no. 1, pp. 543–552, Jan. 2019.

[11] Y. Dong, H. Zhang, and X. Zhang, "On impulse response modeling for underwater wireless optical MIMO links," in *Proc. IEEE/CIC Int. Conf. Commun. China*, 2014, pp. 151–155.

[12] M. Bernotas and C. Nelson, "Probability density function analysis for optimization of underwater optical communications systems," in *Proc. OCEANS MTS/IEEE Washington*, 2015, pp. 1–8.

[13] M. V. Jamali *et al.*, "Statistical distribution of intensity fluctuations for underwater wireless optical channels in the presence of air bubbles," in *Proc. Iran Workshop Commun. Inf. Theory*, 2016, pp. 1–6.

[14] H. M. Oubei *et al.*, "Simple statistical channel model for weak temperature-induced turbulence in underwater wireless optical communication systems," *Opt. Lett*., vol. 42, no. 13, pp. 2455–2458, 2017.

[15] Z. Vali, A. Gholami, Z. Ghassemlooy, M. Omoomi, and D. G. Michelson, "Experimental study of the turbulence effect on underwater optical wireless communications," *Appl. Opt.*, vol. 57, no. 28, pp. 8314–8319, 2018.

[16] M. V. Jamali *et al.*, "Statistical studies of fading in underwater wireless optical channels in the presence of air bubble, temperature, and salinity random variations," *IEEE Trans. Commun*., vol. 66, no. 10, pp. 4706–4723, Oct. 2018.

[17] M. Elamassie and M. Uysal, "Vertical underwater visible light communication links: Channel modeling and performance analysis," *IEEE Trans. Wireless Commun*., vol. 19, no. 10, pp. 6948–6959, Oct. 2020.

[18] M. Mahmoud, A. I. Boghdady, A. E.-R. A. El-Fikky, and M. H. Aly, "Statistical studies using goodness-of-fit techniques with dynamic underwater visible light communication channel modeling," *IEEE Access*, vol. 9, pp. 57716–57725, 2021.

[19] M. V. Jamali *et al.*, "Statistical studies of fading in underwater wireless optical channels in the presence of air bubble, temperature, and salinity random variations," *IEEE Trans. Commun.*, vol. 66, no. 10, pp. 4706–4723, Oct. 2018.

[20] Z. Zeng, S. Fu, H. Zhang, Y. Dong, and J. Cheng, "A survey of underwater optical wireless communications," *IEEE Commun. Surv. Tuts*., vol. 19, no. 1, pp. 204–238, Jan.–Mar. 2017.

[21] N. Saeed, A. Celik, T. Y. Al-Naffouri, and M.-S. Alouini, "Underwater optical wireless communications, networking, and localization: A survey," *Ad Hoc Netw.*, vol. 94, 2019, Art. no. 101935.

[22] L. Bariah, S. Muhaidat, and A. Al-Dweik, "Error probability analysis of non-orthogonal multiple access over nakagami-m fading channels," *IEEE Trans. Commun*., vol. 67, no. 2, pp. 1586–1599, Feb. 2019.

[23] M. Elamassie, L. Bariah, M. Uysal, S. Muhaidat, and P. C. Sofotasios, "Capacity analysis of NOMA-enabled underwater VLC networks," *IEEE Access*, vol. 9, pp. 153305–153315, 2021.

[24] D. Chen, Y. Wang, J. Jin, H. Lu, and J. Wang, "An experimental study of NOMA in underwater visible light communication system," *Opt. Commun*., vol. 475, Nov. 2020, Art. no. 126199.

[25] K. W. S. Palitharathna, H. A. Suraweera, R. I. Godaliyadda, V. R. Herath, and Z. Ding, "Impact of receiver orientation on full-duplex relay aided NOMA underwater optical wireless systems," in *Proc. IEEE Int. Conf. Commun.*, Dublin, Ireland, Jul. 2020, pp. 1–7.

[26] C. Geldard, J. Thompson, and W. O. Popoola, "A study of non-orthogonal multiple access in underwater visible light communication systems," in *Proc. IEEE Veh. Technol. Conf.*, Jun. 2018, pp. 1–6.

[27] C. Geldard, J. Thompson, and W. O. Popoola, "A study of non-orthogonal multiple access in underwater visible light communication systems," in *Proc. IEEE 87th VTC Spring*, 2018, pp. 1–6.

[28] H. Jiang, H. Qiu, N. He, W. Popoola, Z. Ahmad, and S. Rajbhandari, "Performance of spatial diversity DCO-OFDM in a weak turbulence underwater visible light communication channel," *J. Lightw. Technol*., vol. 38, no. 8, pp. 2271–2277, 2020.

[29] M. Abramowitz and I. A. Stegun, *Handbook of Mathematical Functions with Formulas, Graphs, and Mathematical Tables*, 9th ed. New York, NY, USA: Academic Press, 1972.

[30] Z. Ding, Z. Yang, P. Fan, and H. V. Poor, "On the performance of non-orthogonal multiple access in 5G systems with randomly deployed users," *IEEE Signal Process. Lett*., vol. 21, no. 12, pp. 1501–1505, Dec. 2014.

[31] S. Sharma, A. S. Madhukumar, S. R., and C. J. Sheng, "Performance analysis of hybrid FSO/RF transmission for DF relaying system," in *Proc. IEEE Globecom Workshops*, 2017, pp. 1–6.

[32] C. Gabriel, M.-A. Khalighi, S. Bourennane, P. Leon, and V. Rigaud, "Channel modeling for underwater optical communication," in *Proc. IEEE Globecom Workshops*, 2011, pp. 833–837.

[33] C. E. Webb and J. D. Jones, *Handbook of Laser Technology and Applications: Laser Design and Laser Systems*. Boca Raton, FL, USA: CRC Press, 2004.

[34] D. Knuth, "PIN photodetector characteristics for optical fiber communication," [Online]. Available: https://www.fiberoptics4sale.com/blogs/archive-posts/95046662-pin-photodetector-characteristics-for-optical-fiber-communication

[35] J. Grubor, S. Randel, K.-D. Langer, and J. W. Walewski, "Broadband information broadcasting using LED-based interior lighting," *J. Lightw. Technol*., vol. 26, no. 24, pp. 3883–3892, 2008.

[36] M. Cheng, L. Guo, and Y. Zhang, "Scintillation and aperture averaging for Gaussian beams through non-Kolmogorov maritime atmospheric turbulence channels," *Opt. Exp.*, vol. 23, no. 25, pp. 32606–32621, Dec. 2015.

[37] M. Elamassie, M. Uysal, Y. Baykal, M. Abdallah, and K. Qaraqe, "Effect of eddy diffusivity ratio on underwater optical scintillation index," *Opt. Soc. Amer. A*, vol. 34, no. 11, pp. 1969–1973, 2017.